metals

MDPI

Article

Fe-Si/MnZn(Fe_2O_4)$_2$ Core-shell Composites with Excellent Magnetic Properties by Mechanical Milling and Spark Plasma Sintering (SPS)

Liang Yan and Biao Yan *

School of Materials Science and Engineering, Shanghai Key Laboratory of D&A for Metal-Functional Materials, Tongji University, Shanghai 201804, China; 1510446@tongji.edu.cn

* Correspondence: 84016@tongji.edu.cn; Tel.: +86-21-6958-2007

Received: 18 May 2018; Accepted: 29 June 2018; Published: 19 July 2018

Abstract: The Fe-Si/MnZn(Fe_2O_4)$_2$ composite powders are synthetized by means of the mechanical milling, and Fe-Si/MnZn(Fe_2O_4)$_2$ soft magnetic composites are prepared by spark plasma sintering (SPS). The impact of milling time on particle size, phase structure and magnetic properties of the investigative core-shell structure powders along with that of sintering temperature on microstructure and magnetic properties of FeSi-MnZn(Fe_2O_4)$_2$ soft magnetic composite are studied by X-ray diffraction (XRD), scanning electron microscopy (SEM), and vibrating sample magnetometer (VSM). The experimental results demonstrate a layer of MnZn(Fe_2O_4)$_2$ forming a coating on the surface of Fe-Si powder after mechanical milling, and the soft magnetic composites exhibiting excellent magnetic performance at 900 °C: 212.49 emu/g for saturation magnetization, with 6.89 Oe for coercivity, 3×10^{-4} Ω.m for electrical resistivity and stable amplitude permeability and low core loss over a wide frequency range. Therefore, SPS offers a convenient and swift way to enhance performance of soft magnetic composites using magnetic materials as insulting layer.

Keywords: spark plasma sintering; soft magnetic composites (SMCs); microstructures; low core loss

1. Introduction

The soft magnetic composites (SMCs) are described as the electrical insulating materials covering on the surface of ferromagnetic powder particles. They have, in recently years, stolen the limelight resulting from advantages of three-dimensional isotropy (3D), slight eddy current loss, and comparatively mild total loss at medium and high frequencies [1–3]. Generally speaking, the hysteresis loss (Wh), the eddy current loss (We) and the residual loss are entirely composed of the core loss (W) of SMCs [4,5]. As everyone knows, eddy current loss (We) as the main core loss in SMCs causes approximately 10% of electrical energy lose during electromagnetic transmission and distribution at middle and high frequencies. Therefore, the pressing issue has to do with the preparation of SMCs with lower core loss, because the value of We matters to the effective radius of the eddy current (r) and the electrical resistivity (ρ). The use of apposite insulating materials can diminish the radius of the eddy current (r) and advance the electrical resistivity (ρ). As a rule, insulating materials can be classified into organics and in-organics insulating materials. The organics materials, unfortunately, have a limit of heat treatment temperature below 400 °C which leads to a sharp deterioration in magnetic properties and mechanics of SMCs during subsequent annealing process. On the contrary, in-organic insulating materials increase the heat-treatment temperature and improve the properties of SMCs. So far, a number of oxide ceramics, such as SiO_2 [6], ZrO_2 [7] and Al_2O_3 [8], have been perceived as fine insulating materials to reduce core loss in SMCs and improve electrical resistivity. However, due to their non-magnetic with since they are nonmagnetic, they have a tendency to lower saturated magnetic induction density and permeability, and to augment coercivity and hysteresis loss.

The ferrite is a magnetic material which could add saturated magnetic induction density and permeability and also reduce coercivity of the SMCs owing to its high resistance and nice soft magnetic properties when used as an insulting material. Several methods have been utilized for the preparation of such composites powder. Yuandong Peng [9] have synthesized iron/(NiZn)Fe_2O_4 by microwave treatment, and achieved stable permeability and low core loss over a wide frequency range. M. Lauda [10] has prepared FeSi/MnZnFe_2O_4 through sol-gel synthesis together with the auto-combustion process, and gets better soft magnetic properties.

In this paper, the Fe-Si/MnZn-ferrite composite powders with a core-shell structure have been designed. Firstly, the nano-MnZn ferrite particles with fine distribution and purity are synthesized via a sol-gel autocombustion method and relevant details are elucidated in [11]. Soon after, we adopt a way of mechanical milling to make composite powders with MnZn-ferrite powder solely covering on the surface of Fe-Si powders. Besides, the objective powders obtain wonderful magnetic properties with low core loss and high resistivity.

Nevertheless, Fe-Si alloy is highly brittle due to large silicon content and forms ordered phases, such as B2 and DO3 phases, with its ductility to almost zero at room temperature [12,13]. Therefore, it is of crucial importance to develop a novel method to avoid the difficulties caused by the brittleness of Fe-Si alloy apart from the conventional powder metallurgy process. Recently, a new powder metallurgy technique named spark plasma sintering (SPS) characterized by rapid and efficient sinter ceramic, metal ceramic and metal compound nano-materials at low temperature [14–16] has attracted intensive attention. During SPS sintering process, the instantaneous discharge of the plasma causes the particles to uniformly produce Joule heat and activate the particles surface. And plentiful Fe-Si soft magnetic composites like Fe-Si/SiO_2 [17], Fe-Si/MgO [18], have been successfully produced by SPS.

In this paper, the Fe-Si MnZn$(Fe_2O_4)_2$ composite powders are synthetized by means of the mechanical milling, and then Fe-Si/MnZn$(Fe_2O_4)_2$ soft magnetic composites are prepared by SPS. The impact of milling time on fabricate Fe-Si/MnZn$(Fe_2O_4)_2$ composite powders and that of the sintering temperature on the microstructure, magnetic properties of soft magnetic composites are investigated.

2. Experimental

2.1. Materials and Preparation

Raw materials are composed of gas atomized Fe-6.5 wt.% Si (referred to as Fe-Si) powders (commercial purchased) and MnZn$(Fe_2O_4)_2$ powder, (by sol-gel autocombustion described in literature [11]) and the MnZn$(Fe_2O_4)_2$ powder at a ratio of 10 mass%, they are mixed by mechanical milling at a ratary rate of 300 rpm in a planetary ball mill for 0 h, 2 h, 4 h and 8 h, respectively, argon atmosphere is taken during milling process. The composite powders are sintered in a SPS furnace (Model SPS3.20MK-IV, Sumitomo Coal Mining Co., Ltd., Tokyo, Japan) and Figure 1 shows the diagram of SPS sintering pressure of 60 MPa, holding time of 8 min, and sintering temperature varying from 600 °C to 1000 °C. The specimens are sliced to ring cores with the size of 20 mm in outer diameter and 16 mm in inner diameter and 3 mm in thickness, shown in Figure 2. Finally, a raw Fe-Si alloy specimen without any insulating materials was also prepared under the same conditions.

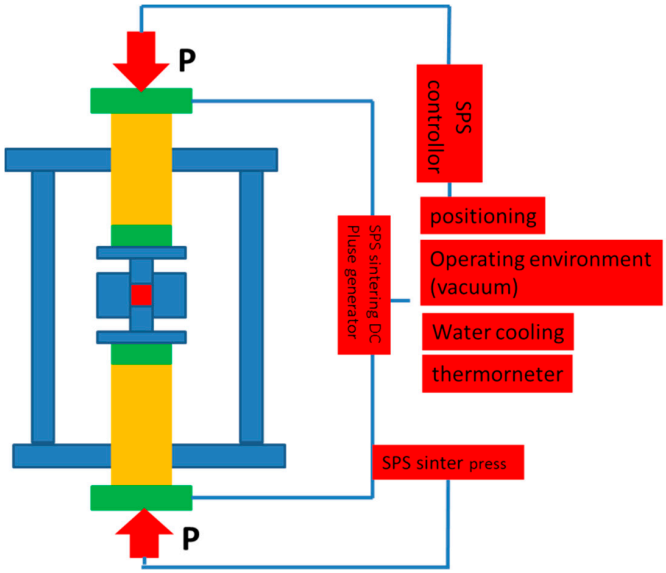

Figure 1. Diagram of spark plasma sintering (SPS) system for preparing composite compacts in this work.

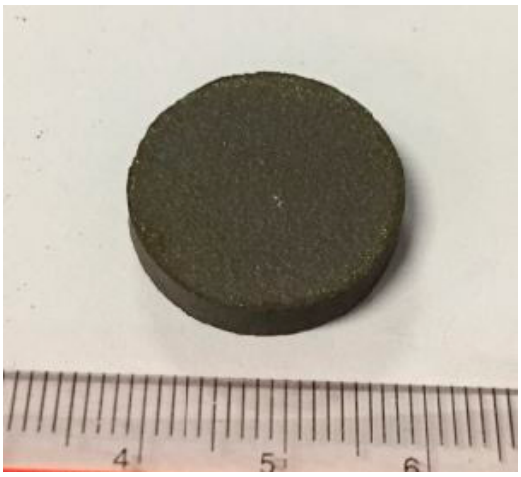

Figure 2. The composite powder cores prepared by SPS.

2.2. Characterizations

The crystalline structure and phase identification are tested by X-ray diffraction (XRD) (DX-2007, Dandong Fang Yuan Co., Ltd., Dandong, China). The morphology and microstructures are characterized by scanning electron microscopy (SEM) (Nova Nano-SEM 450, FEI, Hillsboro, OR, USA) coupled with an energy-dispersive spectroscopy (EDS) (Ultra, EDAX, Mahwah, NJ, USA). The density of the specimens is measured via Archimedes using ethanol as immersion fluid. The static magnetic properties are tested at room temperature using vibrating sample magnetometer (VSM) (Quantum Design, San Diego, CA, USA). Core loss of the ring-shaped magnetic compacts is measured by soft magnetic AC measuring instrument (MATS-2010SA/500k, Linkioin, China).

3. Results and Discussion

3.1. Synthesis of Fe-6.5Si/MnZn(Fe_2O_4)$_2$ Core-Shell Powders

Figure 3 shows the SEM micrographs of the Fe-Si powders with and without coated MnZn(Fe_2O_4)$_2$ powders. It can be observed that the raw Fe-Si powders turn to be spherical and the surface powders are rather smooth (Figure 3a). After the mechanical milling process of covering MnZn(Fe_2O_4)$_2$ powders,

the composite powders become irregularly shaped and relatively rougher (Figure 3c). And we can observe from the magnified image in the selected region of Figure 3d that the Fe-Si powders are evenly coated $MnZn(Fe_2O_4)_2$ powders. According to the principle of EDS generation peak, the coating layer on the surfaces of Fe-Si powders has a certain thickness. The results show that the Fe-Si powder has undergone dramatic mechanical deformation during the milling process on account of the deformation of the powder and the disparate degree of pits on the surface.

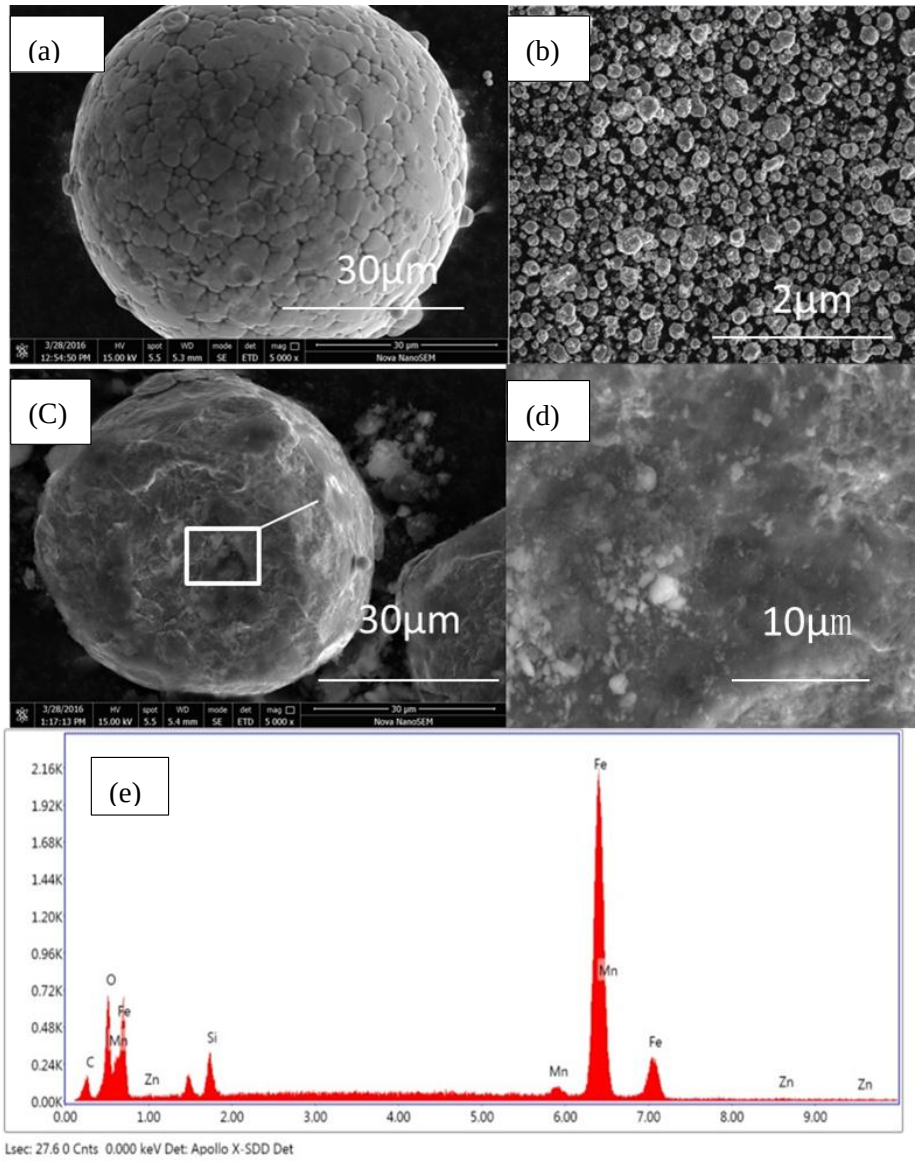

Figure 3. SEM images of (**a**) the raw Fe-Si powders; (**b**) $MnZn(Fe_2O_4)_2$ powders; (**c**) the Fe-Si/$MnZn(Fe_2O_4)_2$ composite powders; (**d**) the magnified image for the selected region in (**c**,**e**) EDS spectrum for the selected region in (**c**).

Figure 4 shows the particle size distribution of raw Fe-Si powder (Figure 4a) and composite powders with a covering of $MnZn(Fe_2O_4)_2$ powders (Figure 4b) and $MnZn(Fe_2O_4)_2$ powders (Figure 4c). It is observed that it is well concentrated and the average diameter of raw Fe-Si powder, composite powders and $MnZn(Fe_2O_4)_2$ powders are 40 μm, 50 μm and 2 μm accordingly. The XRD patterns of the raw Fe-Si powders and the composites powders with various milling times are depicted in Figure 5. As it can be seen from the patterns in Figure 5, there are three characteristic diffraction peaks of the raw Fe-6.5 wt.% Si powder with (110), (200) and (211) of the α-Fe (Si) phases in comparison

with the standard map of the JCPDS card 06-0696. Compared with the XRD pattern of $MnZn(Fe_2O_4)_2$ powders (Figure 6), we can discover that there are new peaks at with 2 degrees at (253), (21), (148) distributed in $MnZn(Fe_2O_4)_2$ phases as expected. We can also draw a conclusion that the $MnZn(Fe_2O_4)_2$ powders merely bonds onto the surface of the Fe-Si powders and the chemical components do not vary through mechanical milling process. In addition, with the augment of the milling time, the width of Fe peaks become more broaden with broader and more weaken with weaker, indicating the powder plastic deformation, increasing tendency of stress, and refining of grain during mechanical milling.

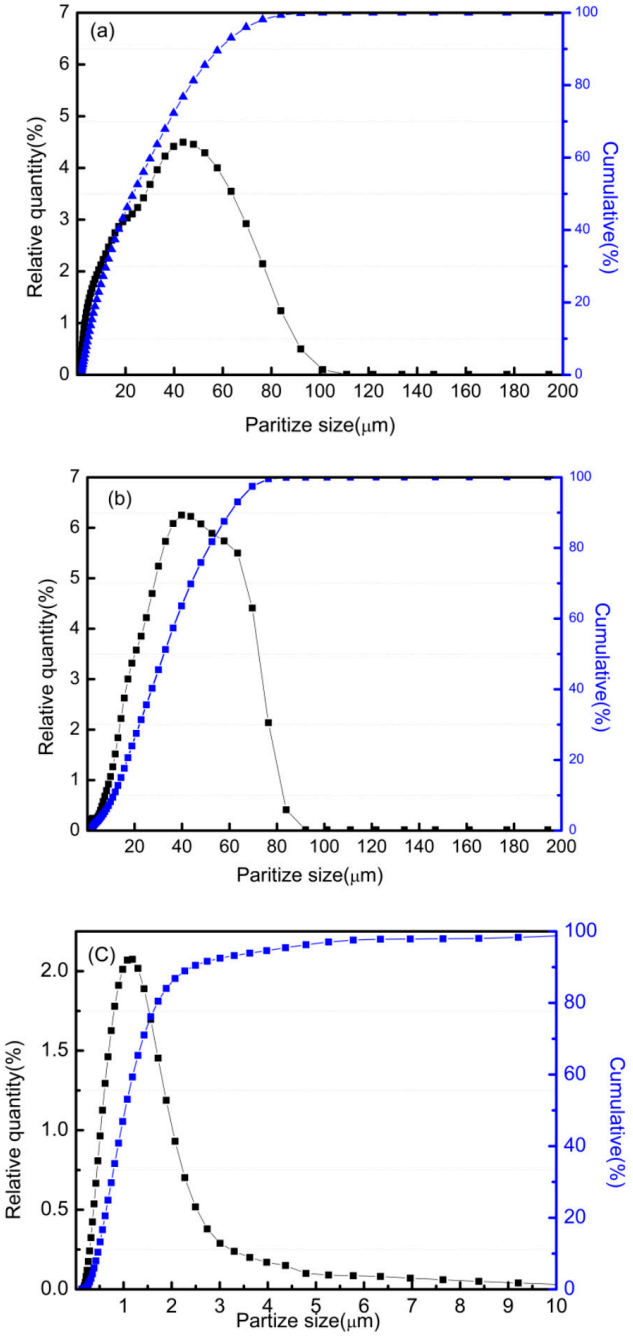

Figure 4. Particle size distribution of the composite powder (**a**) before milling; (**b**) after milling and (**c**) $MnZn(Fe_2O_4)_2$ powders.

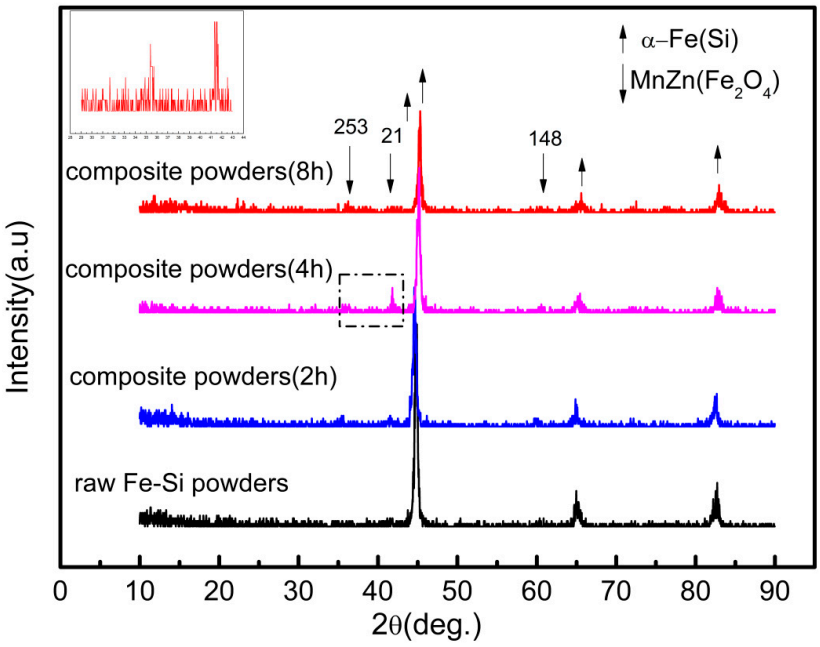

Figure 5. XRD patterns of raw Fe-Si powder and composite powders processed for different milling time (2 h, 4 h, 8 h, respectively).

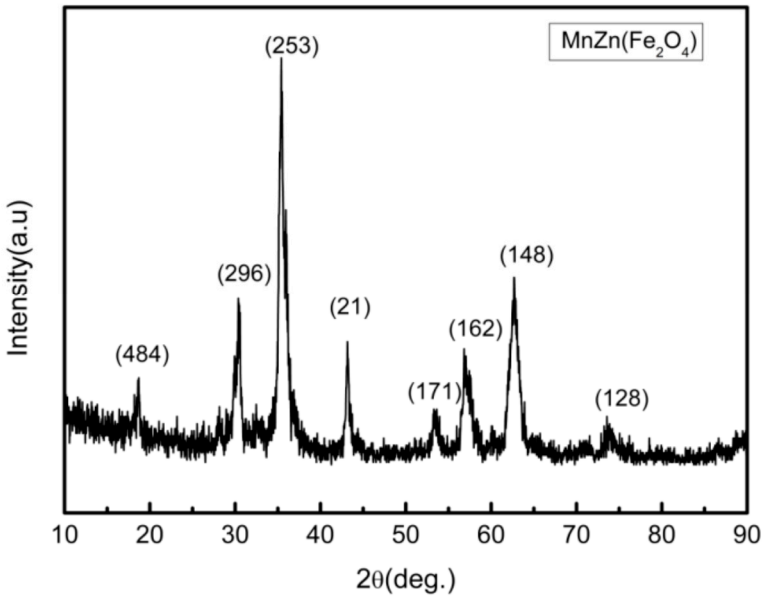

Figure 6. XRD patterns of MnZn $(Fe_2O_4)_2$ powders.

3.2. Magnetic Properties of the Composite Powders

Figure 7 offers us the hysteresis loops of raw Fe-Si powders, $MnZn(Fe_2O_4)_2$ powders and composite powders of different milling time. It can be deduced that the saturation magnetization (Ms) of the composite powders is slightly lower than that of the raw Fe-Si powders. It is mainly because of the composition of Ms which owns a composition and structure in the ferromagnetic phase. Beyond that, the volume fraction of Fe-Si powder is tiny with the presence of the $MnZn(Fe_2O_4)_2$ insulating layer, leading to the reduction of composite powder named Ms. What's more, raising the milling time decreases Ms, implying that agglomeration of the $MnZn(Fe_2O_4)_2$ powder is alleviated, and most are adsorbed on the surface of Fe-Si powder to form a well-coated Fe-Si/$MnZn(Fe_2O_4)_2$ core-shell structure powder.

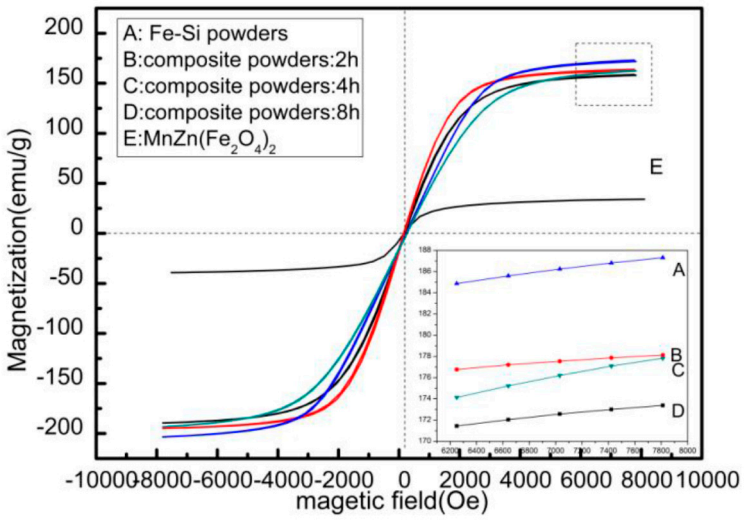

Figure 7. The hysteresis loops of raw Fe-Si powders, $MnZn(Fe_2O_4)_2$ powders and composite powders with different milling time. The inset in figure is the magnified image of the selected region.

Figure 8 mirrors the dependence of coercive force (Hc) for the composite powders with disparate milling time before and after annealing. We can see from it that with augment of milling time, the Hc of composite powders will respectively increase stage by stage. It is because of the accumulation of plentiful internal stress during the milling process, and it results in abundant lattice distortion and crystal defects, pinning of the magnetic domain movement, and the coercivity increase. After annealing, the Hc of composite powders is pretty much lower than that of the milled powder, and it is attributed to the release of internal stress.

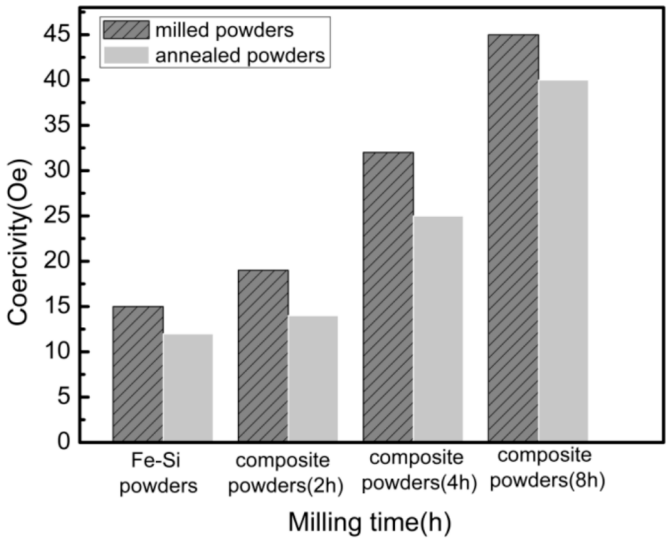

Figure 8. The dependence of coercive force (Hc) for the composite powders with different milling time before and after annealing in argon atmosphere.

3.3. The Microstructure of Fe-Si/MnZn(Fe_2O_4)$_2$ Soft Magnetic Cores(SMCs)

Figure 9 demonstrates that the SEM micrographs of the polished surface of Fe-Si/$MnZn(Fe_2O_4)_2$ composites sinter from 600 °C to 1000 °C. It can also be observed that the dark part is $MnZn(Fe_2O_4)_2$ powder sintered to form a dense and continuous uniformly ceramic cell wall, and the gray part is the Fe-Si powder sintered to form iron-based cell body.

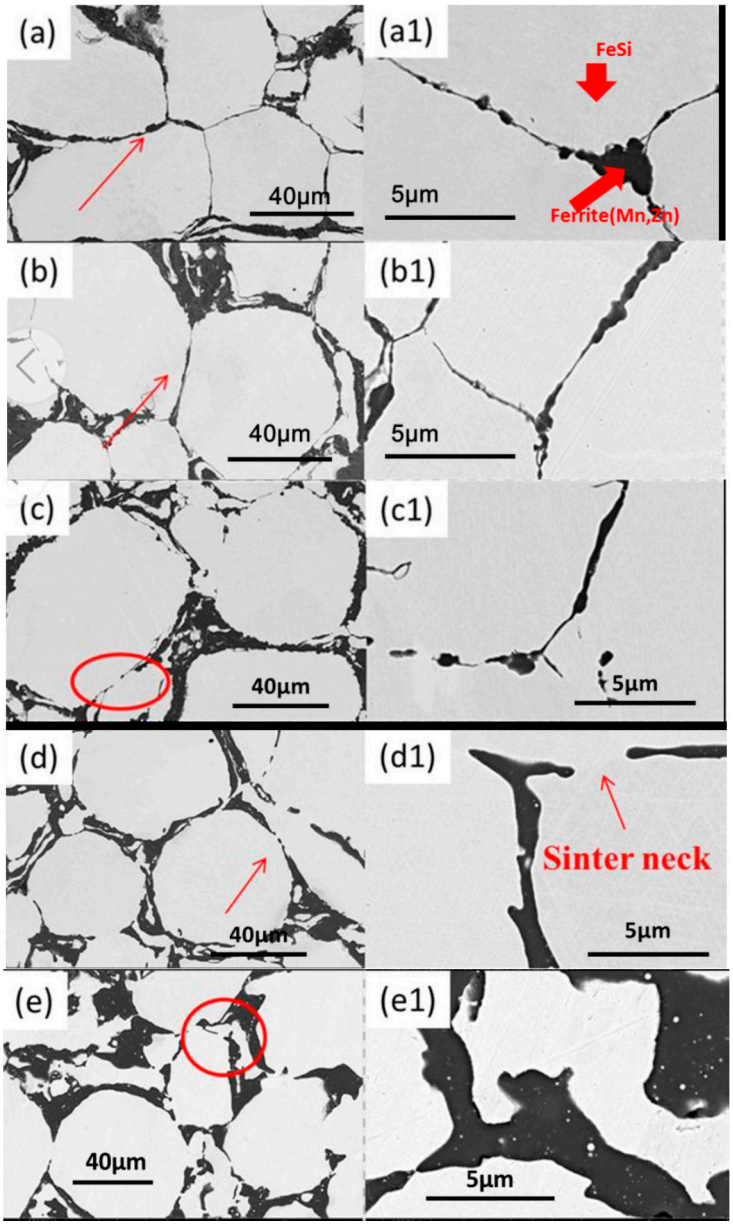

Figure 9. SEM micrographs of the Fe-Si/MnZn(Fe_2O_4)$_2$ composites sintered at different temperatures (no corrosion): (**a**) 600 °C, (**b**) 700 °C, (**c**) 800 °C, (**d**) 900 °C, (**e**) 1000 °C.

In Figure 9a,b, we can find that barely a small quantity of sintered necks is observed, and the FeSi/MnZn(Fe_2O_4)$_2$ particles are identified mainly by mechanical bonding under pressure. It reveals that the FeSi/MnZn(Fe_2O_4)$_2$ alloy has been densified but not sintered. When the sintering temperature increases from 800 °C to 900 °C as showed in Figure 9c,d, the edge of Fe-Si particles become more and more irregular, and the porosity decreases distinctly. It is perceived that the FeSi/MnZn(Fe_2O_4)$_2$ particles undergo plastic deformation under pressure, and the pulse current increases, the Joule heat of particles and the local temperature increases, which gives rise to the melting of FeSi/MnZn(Fe_2O_4)$_2$ particles and the combination. In addition, the formation of sintered neck is greatly reduced when sintering temperature climbs to 1000 °C showed in Figure 9d. Some small Fe-Si particles melt and agglomerate around the large particles, and barely a few large particles are bound to each other to form sintered neck. The number and size of sintered neck is greatly increased, and the insulation of MnZn(Fe_2O_4)$_2$ is destroyed as well. Therefore, FeSi/MnZn(Fe_2O_4)$_2$ alloy at different

sintering temperatures can be divided into three stages: under-firing (600 °C–700 °C), complete sintering (800 °C–900 °C) and over-burning (1000 °C). We can imply from the SEM micrographs of Fe-Si/MnZn(Fe_2O_4)$_2$ composites sintered at 800 °C with EDS in Figure 10 further that Fe-Si powders are well separated and insulated by MnZn(Fe_2O_4)$_2$ layer in the FeSi/MnZn(Fe_2O_4)$_2$ magnetic powder cores and the boundary of the Fe-Si particles exists for all elements (e.g., Fe, Mn, Zn, O).

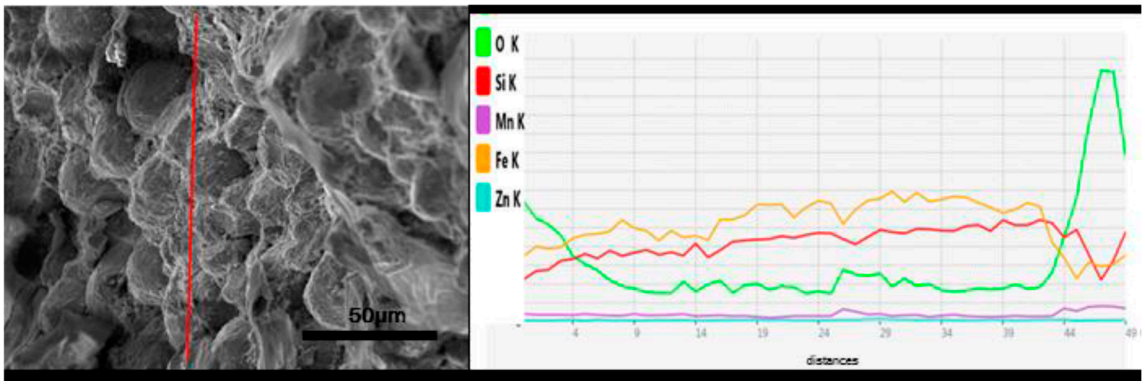

Figure 10. SEM micrographs of the Fe-Si/MnZn(Fe_2O_4)$_2$ composites sintered at 800 °C with EDS analysis (no corrosion).

3.4. The Magnetic Properties of Fe-Si/MnZn(Fe_2O_4)$_2$ Soft Magnetic Cores(SMCs)

Table 1 shows the basic parameters of five specimens, Table 2 summarizes the main magnetic parameters of this study and other study, it is shows that the magnetic properties of our study are superior to the other which using non-magnetic materials as insulating layer. The electrical resistivity of our study is, respectively, 6 and 28 times higher than Fe-Si/SiO_2 and Fe-Si/ZrO_2, It shows that we are able to enhance the electrical resistivity without decreasing the soft magnetic properties using soft magnetic coating in this work.

Table 1. Basic parameters of specimens at different sintering temperatures.

Parameter	Unit	600 °C	700 °C	800 °C	900 °C	1000 °C
External diameter	Φext [mm]	16.94	16.92	16.94	17.01	16.97
Internal diameter	Φint [mm]	11.08	10.75	10.68	11.08	11.23
Height	H [mm]	2.23	1.88	2.02	2.32	2.94
Mass	M [g]	2.6	1.8	1.75	2.3	2.6

Figure 11 exhibits the hysteresis loop of the Fe-Si/MnZn(Fe_2O_4)$_2$ alloy at diverse sintering temperatures from 600 °C to 1000 °C. It can be seen that the sintered block presents unlike magnetization curves during magnetization, and its saturation magnetization Ms change with different sintering temperatures. We use graphics to depict the effects of different sintering temperatures on the saturation magnetization Ms and the coercivity Hc and corresponding variation is shown in Figure 12. There we can find a soft ferromagnetic nature of high saturation magnetization and low coercivityat 900 °C. A similar result is also observed in literatures showing that the Ms value has nothing to do with sintering temperature [19,20].

As illustrated in Figure 12, the value of Ms increase from 184.1 emu/g to 212.5 emu/g with the increase of sintering temperature from 600 °C to 900 °C. However, the Ms value decreases to 188.2 emu/g at 1000 °C. Changes in the Hc value show the opposite trend. The Ms value of the Fe-Si alloy is determined by the intensity of the magnetic iron occupancy, and the magnetic atoms (Mn, Zn) penetrate into the Fe lattice through thermal diffusion with incremental sintering temperature. With the raise of sintering temperature, the density increases (shown in Table 1), the porosity deduces,

and the sum of magnetic moments fortifies, more magnetic atoms (Mn, Zn) are dissolved into Fe, and occupy the gap between the Fe atoms in a certain temperature range (≤900 °C), all of which are conducive to the improvement of Ms value. At the stage of over burning (>900 °C), the exchange of Fe atoms from magnetic atoms (Mn, Zn) causes the Ms value abates. On the other hand, the Hc drops from 18.8 Oe to 6.89 Oe, indicating that the local defects in sintered compacts are ameliorated, such as the release for residual stress [21] and grain growth [22]. Which reduce the pinning sites for domain wall movements and hence brings about the lessening of Hc.

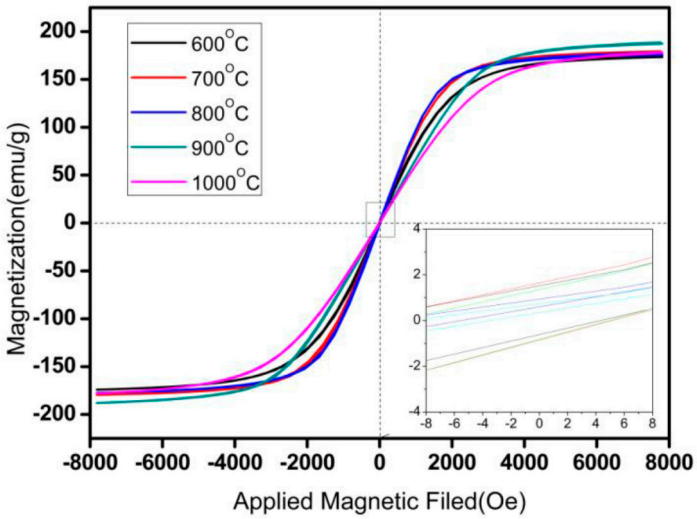

Figure 11. The hysteresis loops of Fe-Si/MnZn(Fe_2O_4)$_2$ composites for different sintering temperatures. The inset in figure is the magnified image of the selected region.

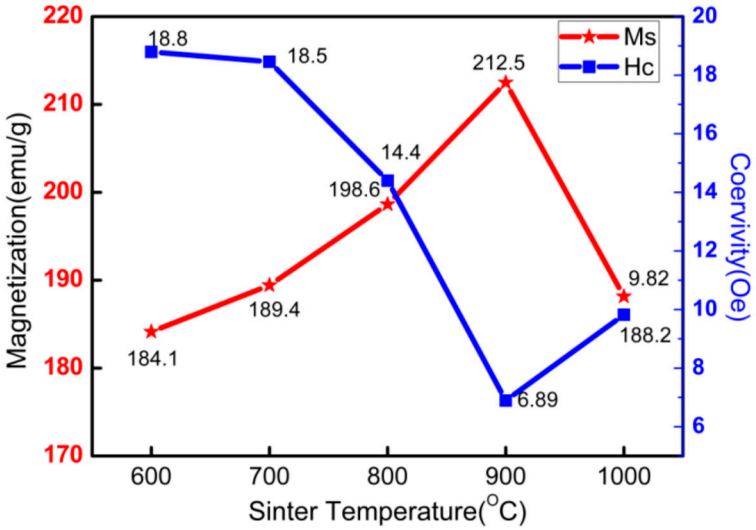

Figure 12. The Fe-Si/MnZn(Fe_2O_4)$_2$ composite of the saturation magnetization (Ms) and coercivity(Hc) values.

Table 2. Main magnetic parameters of our specimens and other study.

Parameter	Ms [emu/g]	Hc [Oe]	ρ [Ω.m]
this study (sintered 900°C)	212.5	6.89	3×10^{-4}
Fe-Si alloy [17]	184.0	10	9.7×10^{-7}
Fe-Si/SiO_2 [17]	164.6	12	4.8×10^{-5}
Fe-Si/ZrO_2 [22]	179.81	20.26	1.066×10^{-5}

Figure 13 manifests the entire core loss versus frequency of the $MnZn(Fe_2O_4)_2$ with coated and uncoated compacts. Compared with the uncoated compacts, the total core loss of coated compacts exhibits a lower value at a high frequency range. Furthermore, the core loss debases evidently with the increasing frequency. Ultimately, the core loss lowers to the minimum values when sintering temperature goes up to 900 °C. It is well known that, the general core loss is the sum of We, Wh and Wr, in which We can be expressed as [23,24]:

$$We = k_e \times (tfB_{max})^2 / \rho$$

where k_e is proportionality constants, B_{max} is the maximum flux density, and t is the thickness of material. Here, We is inversely proportional to the ρ and proportional to the square of the thickness. The remarkable core losses reduction could be ascribed to the insulation effect of $MnZn(Fe_2O_4)_2$ particles. Reasons lie in that it not only significantly boosts the electrical resistivity but also confines the eddy current in the individual Fe-Si particles to enhance the energy conversion efficiency, especially at medium and high frequencies.

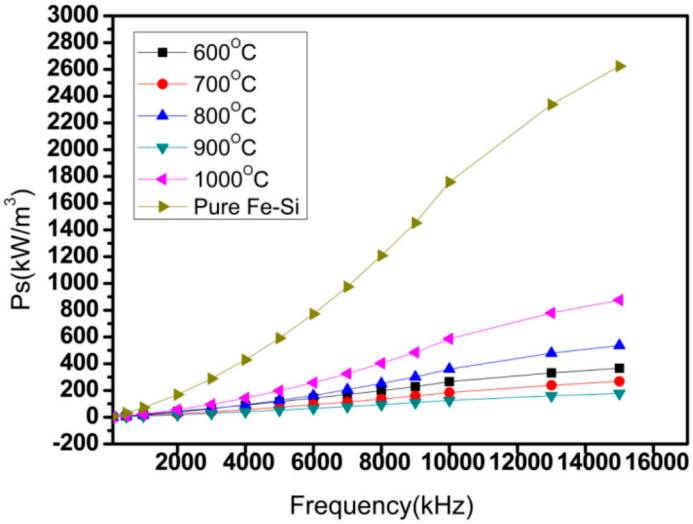

Figure 13. Total core loss as a function of frequency for Fe-Si composite and Fe-Si/$MnZn(Fe_2O_4)_2$ composite with different sintering temperatures measured at maximum induction of 50 mT in the frequency range from 1 kHz to 15 kHz.

Figure 14 shows amplitude permeability of the raw Fe-Si alloy compacts and composite compacts under the same condition that sintered at 900 °C with a frequency range from 1 kHZ to 13 kHz. We can find that the amplitude permeability of Fe-Si alloy compacts shrinks remarkably with the augment of frequencies, but that of the composite compacts is little changed. As we know, the value of the amplitude permeability counts on the density, number of pores, magnetic anisotropy and crystal anisotropy [25,26]. It can be observed in Figure 8 that the Fe-Si particles are segregated by thin MnZn ferrite layer, and the continuous insulating layer become more intact by degrees at 800 °C (shown in Figure 8). The MnZn ferrite between two magnetic particles has analogical function of an air gap so that there is a demagnetizing field in the entire magnetic circuit, resulting in cut of the magnetic permeability. In addition, the powders covering MnZn ferrite have smaller valid particle size and comparatively higher resistivity, which maintain the stable amplitude permeability from low frequencies to high frequencies (measured at 50 mT), explaining that the composite compacts prepared by SPS possess unexceptionable frequency properties.

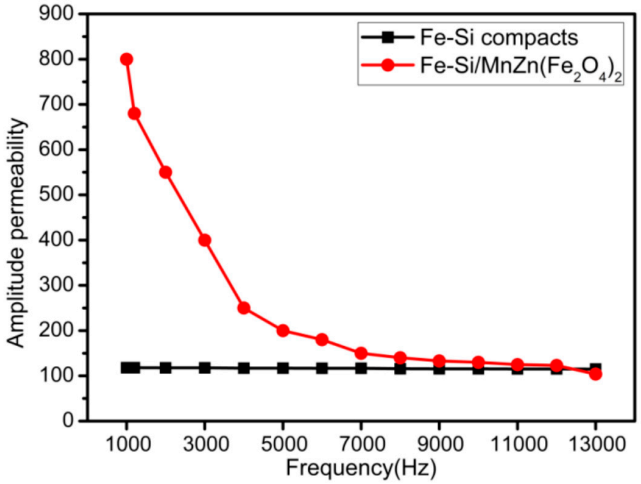

Figure 14. Dependence of amplitude permeability for the Fe-Si composite compacts and Fe-Si/$MnZn(Fe_2O_4)_2$ composite compacts sintered at 900 °C measured at frequency range 1 kHZ to 13 kHZ, B_m = 0.1 T.

4. Conclusions

In this study, $MnZn(Fe_2O_4)_2$ insulating layers are successfully coated on Fe-Si powders by the use of mechanical milling. The composite powders are combined to magnetic powder cores with core-shell structures by SPS. the sintering process of Fe-6.5 wt.% Si/$MnZn(Fe_2O_4)_2$ alloy can be divided into three stages: the under-fire stage (600 °C–700 °C) where composite particle forms machine, the complete sintering stage (800 °C–900 °C) where composite particles Metallurgical combines, and the over-burning stage (1000 °C) where composite particles are melted and agglomerated. We confirm that the Fe-Si/$MnZn(Fe_2O_4)_2$ composite powder cores with 900 °C display excellent soft magnetic properties: Ms of 212.49 emu/g, Hc of 6.89 Oe, high electrical resistivity and stable amplitude permeability and low core loss because of the $MnZn(Fe_2O_4)_2$ insulating layers. These results are superior to other study which takes no-magnetic materials as insulting layer, indicating that SPS is an efficient way of fabricating soft magnetic composites with magnetic materials as insulting layer. And the core-shell structures demonstrate a useful inspiration to reduce core loss and stable permeability over a wide frequency range.

Author Contributions: L.Y. and B.Y. conceived and designed the experiments; L.Y. performed the experiments; L.Y. and B.Y. analyzed the data; B.Y. contributed reagents/materials/analysis tools; L.Y. wrote the paper.

Funding: This work was supported by the National Key Research and Development Program of the 13th Five-Year Plan of China (grant number 2016 Y F B 1200602-02).

Conflicts of Interest: The authors declare no conflicts of interest.

References

1. Shokrollahi, H.; Janghorban, K. Different annealing treatments for improvement of magnetic and electrical properties of soft magnetic composites. *J. Magn. Magn. Mater.* **2007**, *317*, 61–67. [CrossRef]
2. Taghvaei, A.H.; Shokrollahi, H.; Janghorban, K.; Abiri, H. Eddy current and total power loss separation in the iron–phosphate–polyepoxy soft magnetic composites. *Mater. Des.* **2009**, *30*, 3989–3995. [CrossRef]
3. Zhao, G.; Wu, C.; Yan, M. Enhanced magnetic properties of Fe soft magnetic composites by surface oxidation. *J. Magn. Magn. Mater.* **2016**, *399*, 51–57. [CrossRef]
4. Zhang, X.F.; Dong, X.L.; Huang, H.; Liu, Y.Y.; Wang, W.N.; Zhu, B.L.; Lei, J.P. Microwave absorption properties of the carbon-coated nickel nanocapsules. *Appl. Phys. Lett.* **2006**, *89*, 053115. [CrossRef]
5. Mühlethaler, J.; Biela, J.; Kolar, J.W.; Ecklebe, A. Improved Core Loss Calculation for Magnetic Components Employed in Power Electronic System. In Proceedings of the Applied Power Electronics Conference and Exposition, Fort Worth, TX, USA, 6–11 March 2011; Volume 2, pp. 1729–1736.

6. Li, G.Q. Intergranular insulated Fe-6.5 wt% Si/SiO_2 composite compacts with tunable insulating layer thickness for low core loss applications. *J. RSC Adv.* **2015**, *82*, 67031–67040.
7. Soni, K.C.; Chandra, S.S.; Singh, B.; Gopi, T. Catalytic activity of Fe/ZrO_2 nanoparticles for dimethyl sulfide oxidation. *J. Colloid Interface Sci.* **2015**, *446*, 226–236. [CrossRef] [PubMed]
8. Gao, M.; Shi, Z.C.; Fan, R.H.; Qian, L.; Zhang, Z.D.; Guo, J.Y. High-Frequency Negative Permittivity from Fe/Al_2O_3 Composites with High Metal Contents. *J. Am. Ceram. Soc.* **2012**, *95*, 67–70. [CrossRef]
9. Peng, Y.; Nie, J.; Zhang, W.; Bao, C.; Ma, J.; Cao, Y. Preparation of soft magnetic composites for Fe particles coated with $NiZnFe_2O_4$ via microwave treatment. *J. Magn. Magn. Mater.* **2015**, *395*, 245–250. [CrossRef]
10. Lauda, M.; Füzer, J.; Kollár, P.; Strečková, M.; Bureš, R.; Kováč, J.; Bať ková, M.; Bať ko, I. Magnetic properties and loss separation in $FeSi/MnZnFe_2O_4$ soft magnetic composites. *J. Magn. Magn. Mater.* **2016**, *411*, 12–17. [CrossRef]
11. Ebrahimi, S.A.S.; Masoudpanah, S.M. Effects of PH and citric acid content on the structure and magnetic properties of MnZn ferrite nanoparticles synthesized by a sol-gel autocombustion method. *J. Magn. Magn. Mater.* **2014**, *357*, 77–81. [CrossRef]
12. Lima, C.C.; Silva, M.C.A.D.; Sobral, M.D.C.; Coelho, R.E.; Bolfarini, C. Effects of order–disorder reactions on rapidly quenched Fe-6.5wt.%Si alloy. *J. Alloys Compd.* **2014**, *586*, S314–S316. [CrossRef]
13. Romaric, C.; Le, G.S.; Foad, N.; Frédéric, C.; Guillaume, B.; Gilbert, F.; Jean-Marc, C.; Frédéric, B. Effect of current on the sintering of pre-oxidized copper powders by SPS. *J. Alloys Compd.* **2017**, *692*, 478–484. [CrossRef]
14. Lu, X.; Liang, G.; Sun, Q.; Yang, C. High-frequency magnetic properties of $FeNi_3$-SiO_2 nanocomposite synthesized by a facile chemical method. *J. Alloys Compd.* **2011**, *509*, 5079–5083. [CrossRef]
15. Wu, S.; Sun, A.; Xu, W.; Zou, C.; Yang, J.; Dong, J. Magnetic properties and loss separation in iron-silicone-MnZn ferrite soft magnetic composites. *Am. Inst. Phys.* **2013**, *1569*, 458–461.
16. Wang, M.; Zan, Z.; Deng, N.; Zhao, Z. Preparation of pure iron/Ni-Zn ferrite high strength soft magnetic composite by spark plasma sintering. *J. Magn. Magn. Mater.* **2014**, *361*, 166–169. [CrossRef]
17. Wu, Z.; Fan, X.A.; Wang, J.; Li, G.; Gan, Z.; Zhang, Z. Core loss reduction in Fe-6.5wt.%Si/SiO_2 core-shell composites by ball milling coating and spark plasma sintering. *Alloys Compd.* **2014**, *617*, 21–28. [CrossRef]
18. Qu, X.-J.; Zhao, Z.K. Fe-6.5wt.%Si/MgO Micri-celluler Soft Magnetic Composites (SMCs) prepared with So-gel and SPS. *Changchun Gongye Daxue Xuebao Ziran Kexueban* **2015**, *36*, 130–133.
19. Al-Ali, S.; Oshida, Y.; Andres, C.J.; Barco, M.T.; Brown, D.T.; Hovijitra, S.; Ito, M.; Nagasawa, S.; Yoshida, T. Effects of coupling methods on galvanic corrosion behavior of commercially pure titanium with dental precious alloys. *Biomed. Mater. Eng.* **2005**, *15*, 307–316. [PubMed]
20. Shen, B.; Kimura, H.; Inoue, A.; Omori, M.; Okubo, A. Bulk Amorphous, NanoCrystalline and Nano-Quasicrystalline Alloys. IV. Preparation of $Fe_{65}Co_{10}Ga_5P_{12}C_4B_4$ Bulk Glassy Alloy with Good Soft Magnetic Properties by Spark-Plasma Sintering of Glassy Powder. *Mater. Trans.* **2002**, *43*, 1961–1965. [CrossRef]
21. Wu, C.; Chen, H.; Lv, H.; Yan, M. Interplay of crystallization, stress relaxation and magnetic properties for FeCuNbSiB soft magnetic composites. *J. Alloys Compd.* **2016**, *673*, 278–282. [CrossRef]
22. Geng, K.; Xie, Y.; Yan, L.; Yan, B. Fe-Si/ZrO_2 composites with core-shell structure and excellent magnetic properties prepared by mechanical milling and spark plasma sintering. *J. Alloys Compd.* **2017**, *718*, 53–62. [CrossRef]
23. Shokrollahi, H.; Janghorban, K. Soft magnetic composite materials (SMCs). *J. Mater. Process. Technol.* **2007**, *189*, 1–12. [CrossRef]
24. Li, X.; Makino, A.; Kato, H.; Inoue, A.; Kubota, T. $Fe_{76}Si_{9.6}B_{8.4}P_6$ glassy powder soft-magnetic cores with low core loss prepared by spark-plasma sintering. *J. Mater. Sci. Eng. B* **2011**, *176*, 1247–1250. [CrossRef]
25. Gilbert, I.; Bull, S.; Evans, T.; Jack, A.; Stephenson, D.; Sa, A.D. Effects of processing upon the properties of soft magnetic composites for low loss applications. *J. Mater. Sci.* **2004**, *39*, 457–461. [CrossRef]
26. Shokrollahi, H.; Janghorban, K.; Mazaleyrat, F.; Bue, M.L.; Ji, V.; Tcharkhtchi, A. Investigation of magnetic properties, residual stress and densification in compacted iron powder specimens coated with polyepoxy. *Mater. Chem. Phys.* **2009**, *114*, 588–594. [CrossRef]